HOKKAIDO UNIVERSITY

Title	Directed Evolution and Structural Analysis of NADPH-Dependent Acetoacetyl Coenzyme A (Acetoacetyl-CoA) Reductase from Ralstonia eutropha Reveals Two Mutations Responsible for Enhanced Kinetics
Author(s)	Matsumoto, Ken'ichiro; Tanaka, Yoshikazu; Watanabe, Tsuyoshi; Motohashi, Ren; Ikeda, Koji; Tobitani, Kota; Yao, Min; Tanaka, Isao; Taguchi, Seiichi
Citation	Applied and environmental microbiology, 79(19), 6134-6139 https://doi.org/10.1128/AEM.01768-13
Issue Date	2013-10
Doc URL	http://hdl.handle.net/2115/55134
Type	article (author version)
File Information	finaldraft.pdf

Instructions for use

Hokkaido University Collection of Scholarly and Academic Papers : HUSCAP

Directed evolution and structural analysis of NADPH-dependent acetoacetyl-CoA reductase from *Ralstonia eutropha* reveals two mutations responsible for enhanced kinetics

Ken'ichiro Matsumoto[‡1¶], Yoshikazu Tanaka[§1+], Tsuyoshi Watanabe[‡1¶], Ren Motohashi[‡1], Koji Ikeda[§], Kota Tobitani[‡], Min Yao[§+], Isao Tanaka[§+], and Seiichi Taguchi[‡¶#]

from the [‡]Division of Biotechnology and Macromolecular Chemistry, Graduate School of Engineering, [¶]Japan Science and Technology Agency, CREST, 4-1-8 Honcho Kawaguchi, Saitama 332-0012, Japan, and [§]Graduate School of Life Sciences, and [+]Faculty of Advanced Life Sciences,, Hokkaido University, N13-W8, Kita-ku, Sapporo 060-8628, Japan

*****Running title: *Evolved NADPH-dependent acetoacetyl-CoA reductase*

[1] The first four authors equally contributed to the present study.

[#] To whom correspondence should be addressed: Div. of Biotechnology and Macromolecular Chemistry, Graduate School of Engineering, Hokkaido University, N13-W8, Kita-ku, Sapporo 060-8628, Japan. Tel.: +81-11-706-6610; Fax: +81-11-706-6610; E-mail: staguchi@eng.hokudai.ac.jp

Keywords: in vitro evolution; polyhydroxyalkanoate; biobased plastic; 3-ketoacyl-ACP reductase

ABSTRACT

Nicotinamide adenine dinucleotide phosphate (NADPH)-dependent acetoacetyl-CoA reductase (PhaB) is a key enzyme in the synthesis of poly(3-hydroxybutyrate) [P(3HB)], along with β-ketothiolase (PhaA) and polyhydroxyalkanoate synthase (PhaC). In this study, PhaB from *Ralstonia eutropha* was engineered by means of directed evolution consisting of an error-prone PCR-mediated mutagenesis and a P(3HB) accumulation-based *in vivo* screening system using *Escherichia coli*. Out of approximately twenty thousand mutants, we obtained two mutant candidates bearing Gln47Leu (Q47L) and Thr173Ser (T173S) substitutions. The mutants respectively exhibited a 2.4 and 3.5-fold higher k_{cat} value compared to that of wild-type enzyme. In fact, the PhaB mutants did exhibit enhanced activity and P(3HB) accumulation when expressed in recombinant *Corynebacterium glutamicum*. Comparative three-dimensional structural analysis between the wild-type and highly active PhaB mutants revealed that the beneficial mutations affected the flexibility around the active site, which in turn play an important role in substrate recognition. Furthermore, both the kinetic analysis and crystal structure data supported the conclusion that PhaB forms a ternary complex with NADPH and acetoacetyl-CoA. These results suggest that the mutations affected the interaction with substrates, resulting in the acquirement of enhanced activity.

INTRODUCTION

Nicotinamide adenine dinucleotide phosphate (NADPH)-dependent acetoacetyl-CoA (AcAcCoA) reductase (PhaB) stereoselectively reduces the 3-ketone group of acetoacetyl-CoA so as to synthesize (*R*)-3-hydroxybutyryl(3HB)-CoA, which is known to be a monomer precursor of microbial polyester polyhydroxyalkanoate (PHA) (1-3). The PhaB-encoding gene is found in many bacteria, including *Ralstonia eutropha* (also known as *Cupriavidus necator*), and typically located in the *phb* operon together with β-ketothiolase (PhaA) and PHA synthase (PhaC). The three enzymes catalyze the successive reactions synthesizing P(3HB) from acetyl-CoA (4-5). This pathway has been extensively utilized for the microbial production of P(3HB) and 3HB-based copolymers (6), both of which can be used as biobased plastics. For efficient production of these polymers, the enhancement in the activities of these enzymes is effective (7-8). In several cases, it has been known that the enhanced expression of either PhaB by itself or both PhaA and PhaB increased P(3HB) production by as the result of an increase in gene dosage (9) and codon optimization (10).

There are two major strategies to engineer enzymes for acquiring enhanced activity; structural and non-structural approaches. The three-dimensional structure of PhaB has not been determined, despite its important role in PHA biosynthesis. PhaB possesses a primary structure that is similar to NADPH-dependent 3-ketoacyl-acyl-carrier-protein(ACP) reductase (FabG), which generates the (*R*)-3-hydroxyacyl-ACP involved in fatty acid biosynthesis. However, although PhaB and FabG presumably have similar protein folding and reaction mechanisms to some extent, the regions contributing to the activity of PhaB and FabG have not been identified. Thus, at present we still do not have sufficient

information to design the structure-based engineering of PhaB for the activity enhancement.

Therefore, at the initial step in the present study, we attempted to enhance the enzymatic activity of PhaB using a non-structural strategy of a random mutagenesis of PhaB and high-throughput screening of the activity-enhanced PhaB mutants. This method is applicable without structural information, and is a useful means of identifying regions which exert an effect on the enzymatic activity. In the next step, the wild-type (WT) PhaB and certain highly active mutants were subjected to crystal structure analysis. The structural features of the beneficial sites and comparative analysis of the structure of the WT and activity-enhanced mutants were expected to provide insight into the regions in PhaB contributing to the reaction rate as well as the reaction mechanism of this enzyme.

A technical barrier impeding this goal had been the design of a high-throughput screening method for selecting highly active PhaB mutants. Our group has performed extensive *in vitro* evolution of PhaC for the purposes of increasing its activity (11-12) and altering its substrate specificity (13-14). The *in vivo* screening method used in these studies is based on polymer accumulation in recombinant *Escherichia coli* expressing the randomly mutated *phaC* gene together with the *phaAB* genes, and grown on Nile red-containing agar plates (15-17). The presence of Nile red-stained hydrophobic polymer granules in the cells allowed visualization of the polymer content in terms of the relative fluorescent intensity of the colonies. Namely, the colonies with a brighter fluorescence were suggested to be highly active mutants of the targeted enzyme. However, this method was not exclusively applicable to the engineering of PhaB, because the activity of the WT

PhaB achieved approximately 60 wt% polymer accumulation in *E. coli* (15, 17), which resulted in the saturated fluorescence and prevented the selection of mutants with a higher activity. Thus, the optimizing condition of the plate assay should allow for easy identification of the positive candidates from the other mutants and even the WT enzyme.

To meet this challenge, we replaced PhaA with AcAc-CoA synthase (AACS), which was recently isolated from terpenoid-producing *Streptomyces* sp. strain CL190 (18). AACS acted as a less efficient AcAc-CoA supplying enzyme than PhaA, and recombinant *E. coli* harboring the *AACS* gene, together with the WT *phaB* and *phaC* genes, accumulated a small amount of P(3HB) (19). The low basal polymer accumulation level, i.e. the weak fluorescence in the colonies expressing the WT *phaB* gene, would be preferable for isolating colonies emitting a brighter fluorescence. In fact, this approach successfully retrieved highly active mutants of PhaB. The kinetics and crystal structure of the obtained mutants are discussed.

MATERIALS AND METHODS

Plasmid constructions and screening of *phaB* gene. The *phaB* gene of *R. eutropha* was amplified under error-prone conditions (20) using pGEM"CAB as a template and a pair of primers, 5'-TTCCGGGGCTCGAGCGGTTG-3' and 5'-CTCAAGCTAGCATGCAACG-3'. The restriction sites used for the construction are underlined. The amplified fragment was digested with *Xho*I/*Eco*T22I and inserted into *Xho*I/*Eco*T22I sites of pGEM"CAACSB, which harbors AcAc-CoA synthase gene (*AACS*) together with the *phaB* and *phaC* genes (19) to replace the *phaB* gene with its mutants. The

plasmids were introduced into *E. coli* JM109 and cells were grown on LB agar plates containing glucose and Nile red (20). Colonies emitting enhanced fluorescence on a transilluminator were chosen as potential mutants of high activity.

To express the selected *phaB* mutant genes in *C. glutamicum*, the plasmids pPS*CAB*(Q47L) and pPS*CAB*(T173S) were constructed as follows. The *AACS* gene in the selected pGEM"CAACSB was replaced with the *phaA* gene from *R. eutropha* using the *Pst*I/*Xho*I sites. The resultant plasmids pGEM"*phaCAB*(Q47L) and pGEM"*phaCAB*(T173S) were digested with *Csp*45I/*Bam*HI, and a 4.3-kb fragment was inserted into the *Bst*EII/*Bam*HI site of pPSPTG1 harboring the *cspB* promoter (21) to yield pPS*CAB*(Q47L) and pPS*CAB*(T173S), respectively. pPS*CAB* (21) bearing the WT *phaB* gene was used as a control.

For enzyme purification, the selected *phaB* gene mutants as well as the wild-type gene were amplified using a pair of primers; 5'-GTGGGATCCACTCAGCGCATTGCG-3' and 5'-GCCAAGCTTTCAGCCCATATGCAG-3'. The restriction sites used for the construction are underlined. The amplified fragments were digested with *Bam*HI/*Hin*dIII and inserted into pQE30 (Qiagen, USA) to construct the gene encoding the N-terminal His-tag fusion of PhaB (pQEphaB).

Polymer productions and analysis. For polymer production in *E. coli*, the engineered cells harboring pGEM"CAACSB were grown on LB medium containing 2% glucose and 100 μg/L ampicillin at 37°C for 48 h. Cells were lyophilized and the P(3HB) content was determined by HPLC, as described previously (22).

Transformation of *C. glutamicum* ATCC 13803 was performed by electroporation, as

described previously (21). The recombinant cells harboring pPS*CAB*(WT, Q47L and T173S) were grown on CM2G medium at 30°C for 12 h, then transferred into MMTG medium (23) containing 6% glucose and further cultivated at 30°C for 72 h. P(3HB) content was determined by HPLC, as described (22).

PhaB activity in crude extract. The PhaB activity in the crude extract of *C. glutamicum* harboring pPS*CABs* was measured as well. Cells grown on MMTG medium under the same condition for P(3HB) production were harvested at 24 h. The both cells were suspended in 125 mM Tris-HCl buffer (pH 8.0) and disrupted by sonication. The soluble fraction was used for enzymatic assay. The reaction mixture contained 125 mM Tris-HCl buffer (pH 8.0), 5 mM AcAc-CoA (SIGMA), 20 mM NADPH (Oriental Yeast Co., LTD, Japan) and 3.125% (vol./vol.) crude extract. The decrease in absorbance at 340 nm was monitored at 30°C to measure the consumption rate of NADPH. The activity was normalized by the protein concentration determined using Bradford assay (Biorad).

Purification of PhaB and kinetic analysis. *E. coli* BL21(DE3) harboring pQEphaB (the WT and mutants) and pREP4 bearing *lacI* repressor gene (Qiagen, USA) was grown on LB medium containing 100 μg/L ampicillin and 25 μg/L kanamycin at 25°C for 2.5 h. Then a final 1.0 mM IPTG was added and cells were further cultivated for 10 h. Purification of the N-terminal His-tag fusion of PhaB was performed using His-Bind Resin (Novagen), as described previously (24). The eluted solution was replaced with 20 mM Tris-HCl (pH 8.0) containing 200 mM NaCl using a PD10 column (GE Healthcare) and stored at -80°C until analysis. The assay was carried out at 30°C using 125 mM Tris-HCl (pH 8.0) containing 130 - 180 ng enzyme, and varied concentrations of AcAc-CoA (4.2 to

12.5 μM) and NADPH (25 to 125 μM).

Crystallization and structural analysis. The His-tag fusion of PhaB was further purified on a HiLoad 26/60 Superdex 200-pg column (GE Healthcare) pre-equilibrated with 20 mM Tris-HCl (pH 8.0) and 200 mM sodium chloride. The crystals of PhaB were obtained from a buffer containing 0.1 M MES (pH 7.1), 1.6 M ammonium sulfate and 10% 1,4-dioxane. Crystals of PhaB complexed with $NADP^+$ and AcAc-CoA were obtained from the same buffer containing 0.9 mM $NADP^+$ and 0.9 mM AcAc-CoA. Crystals of the Q47L mutant and T137S mutant were grown from a buffer composed of 0.6 – 1.2 M sodium / potassium tartrate, 0.16 – 0.20 M lithium sulfate and 0.1 M CHES (pH 8.9 – 9.9). X-ray diffraction experiments were performed at SPring-8 (Harima, Japan) and Photon Factory (Tsukuba, Japan) under the proposal number of 2010B1460 and 2011G012, respectively. The X-ray diffraction data set was collected under cryogenic conditions (100 K). Crystals were soaked in a mother liquor containing 20% glycerol and flash-cooled in a stream of liquid nitrogen. The diffracted data were indexed, integrated and scaled using the HKL2000 program package (25) or the XDS (26). The statistical data are shown in Table S1.

The structure of PhaB was determined by the molecular replacement method by means of the MOLREP program (27) using the structure of FabG from *E. coli* (PDB ID 1I01) as the search probe. To monitor the refinement, a random 5% subset was set aside for calculation of the R-free factor. After several cycles of manual model fitting and building with Coot (28) and refinement with REFMAC5 (29), individual atomic coordinate refinement and individual ADP refinement were performed using phenix.refine (30). The

atomic coordinates of WT PhaB, mutant and ternary complex have beendeposited in the Protein Data Bank, www.pdg.org (PDB ID codes 3VZP, 3VZR, and 3VZS). The refinement statistical data are summarized in Table S1.

Particle size analysis. The PhaB particle size in solution was analyzed with dynamic light scattering (DLS) using a Zetasizer Nano-ZS (Malvern). PhaB at 5 mg/ml was filtered and then analyzed.

RESULTS

Selection of beneficial PhaB mutants from the mutant library. Recombinant *E. coli* harboring the mutagenized *phaB* gene, together with the *AACS* and *phaC* genes, were grown on Nile red-containing plates for the screening of beneficial PhaB mutants. Out of the approximately twenty thousand mutant clones, we isolated two colonies emitting a brighter fluorescence. The selected mutants produced 7.0 ± 0.3 and 6.8 ± 0.2 wt% P(3HB), respectively, while the WT produced 6.0 ± 0.3 wt% under the same conditions. These results suggest that the selected mutants were highly active. The gene sequence of the mutants revealed that the PhaB mutants bore Gln47Leu (Q47L) and Thr173Ser (T173S) substitutions, respectively.

Enhanced P(3HB) production using highly active PhaB mutants in engineered *C. glutamicum*. The effect of the selected PhaB mutants on *in vivo* P(3HB) production was evaluated using *C. glutamicum*, which is a GRAS (Generally Recognized As Safe) platform for microbial polyester production (21, 31), because P(3HB) accumulation in recombinant *E. coli* expressing the wild-type *phaCAB* genes was close to saturation (15,

17). Indeed, the recombinant *C. glutamicum* harboring the two mutants exhibited increased P(3HB) accumulation (Fig. 1A) and the PhaB activities were correlated with the polymer content (Fig. 1B). This result indicated that the selected PhaB mutants were highly active and exerted a beneficial effect on P(3HB) production in the *C. glutamicum* strain.

The PhaB mutants exhibited an enhanced turnover rate. The kinetics of the selected mutants was analyzed using the N-terminal His-tag fusion forms of PhaB and its mutants expressed in *E. coli*. The homogeneously purified PhaB and its mutants using one step Ni-column affinity chromatography were directly used in the analysis. The activity of the recombinant PhaB and its mutants was measured using the varied concentrations of the two substrates, AcAc-CoA and NADPH. The kinetic parameters of PhaBs were determined (Table 1) based on Lineweaver–Burk plots (Fig. S1). The Q47L and T173S mutants had 2.4 and 3.5-fold higher k_{cat} values than the WT enzyme, respectively. The increase in k_{cat} was associated with increases in the $K_{M(NADPH)}$ and $K_{M(AcAcCoA)}$ values. The k_{cat}/K_M values of the Q47L mutant were elevated for $k_{cat}/K_{M(NADPH)}$, while $k_{cat}/K_{M(AcAcCoA)}$ was lower than that of WT PhaB. In contrast, the $k_{cat}/K_{M(AcAcCoA)}$ value of T173S was higher than the WT, although $k_{cat}/K_{M(NADPH)}$ was decreased by this mutation. These results suggest that the effects of the two mutations on the interaction between the enzyme and the two kinds of substrates were different. Namely, the Q47L mutation may improve the recognition of NADPH rather than AcAc-CoA, while T173S may contribute to the AcAc-CoA recognition. In addition, kinetic analysis provided insight into the reaction mechanism. The lines produced from the Lineweaver–Burk plot intersected (Fig. S1), suggesting that PhaB had a ternary-complex rather than a ping–pong mechanism.

198

199 **Crystal structure analysis of PhaB and certain highly active mutants.** In order to
200 obtain a better understanding of the beneficial mutation effects, the PhaB crystal structure
201 was determined at a resolution of 1.8 Å by a molecular replacement method using the
202 structure of 3-ketoacyl-ACP reductase (FabG) as a search probe. Four molecules of PhaB
203 were contained in an asymmetric tetramer with the point group being 222, which was
204 observed also for FabG (Fig. 2A and B). The tetramer of PhaB was superimposed onto the
205 tetrameric FabG, with an RMSD of 1.85 Å for the 865 Cα atoms (Fig. S1). DLS analysis
206 revealed a radius of approximately 43.6 Å for PhaB in solution, which is in good
207 agreement with the tetrameric structure in the crystal. These observations indicated that
208 PhaB exists as a tetramer in solution, as is the case for FabG.

209 The crystal structures of the Q47L and T173S mutants were determined at a resolution
210 of 2.0 and 2.9 Å, respectively. A single asymmetric unit contained two molecules, and
211 these formed a crystallographically evident tetramer. The tetrameric structures of these
212 mutants were superimosable onto that of the WT PhaB (0.62 Å for the 974 Ca atoms of
213 Q47L and 0.71 Å for the 975 Ca atoms of T173S), although the α7 – 8 regions and their
214 continuous loops exhibited conformational changes (Fig. 2C). The temperature factor of
215 the α7 – 8 regions of the WT structure were significantly high compared with other regions
216 (Fig. 2D), suggesting that this region has an intrinsically flexible characteristic. DLS
217 analysis revealed a radius of 44.8Å and 44.5 Å for the Q47L and T173S mutants,
218 respectively, clearly indicating that each of these mutants formed a tetramer in solution.
219 Taken together, it can be concluded that these mutants maintained a tetramer structure that

220 was identical to the WT enzyme, and thus there is a reason other than drastic structural
221 change for the increase in the enzymatic activity due to these mutations.

222 PhaB formed a ternary complex with AcAc-CoA and NADPH. In order to obtain an
223 understanding of the contribution of the mutations to the enzymatic activity, the crystal
224 structure of PhaB in complex with AcAc-CoA and $NADP^+$ was determined. In the structure
225 obtained, an obvious electron density pattern corresponding to these substrates was
226 observed in a large cavity found in all four molecules in a single asymmetric unit, and both
227 $NADP^+$ and AcAc-CoA were present (Fig. 3A and B). This structure strongly supports the
228 finding that the reaction mechanism is effected via a ternary complex as proposed by the
229 kinetic analysis.

230 The $NADP^+$ molecule was bound non-covalently in the cavity encircled by loops
231 between β1 – α1, β 2 – α2, β3 – α3, β4 – α4, β5 – α5 and β6 – α7. The corresponding
232 region of FabG was also used for the NADP(H)-binding pocket (32). $NADP^+$ was directly
233 recognized by Arg40, Gly60-Asn61, Gly90-Thr92 and Pro183-Val191 (Fig. 3C). It should
234 be noted that Pro183-Val191 corresponds to α8 and its continuous loop, which exhibits
235 flexibility in the apo form (Fig. 2C and D).

236 An AcAc-CoA molecule was found adjacent to the $NADP^+$ binding site. The
237 nicotinamide ring of $NADP^+$ was in contact with the AcAc moiety, which explains the
238 catalytic reduction of AcAc-CoA. AcAc-CoA is recognized by Ser140, Thr92, Asp94,
239 Gln147-Tyr153, Gly184, Tyr185 and Arg195. Gly184, Tyr185 and Arg195 are located in a
240 flexible portion of α7 – 8 (Fig. 2C, D, Fig. 3C, and D), suggesting that the flexibility of
241 this region may have a significant role in both AcAc-CoA and NADP(H) recognition.

Discussion

The kinetic analysis indicated that the T173S mutant exhibited a higher $k_{cat}/K_{M(AcAcCoA)}$ than the WT PhaB, whereas $k_{cat}/K_{M(NADPH)}$ was lower than the WT. This result shows that the reaction with AcAc-CoA was accelerated by the T173S mutation. This effect was interpreted based on the crystal structure. The residue at the beneficial site 173 of the adjacent subunit (subunit A) was shown to be located close to the adenylyl moiety of AcAc-CoA, although direct interaction was not observed (Fig. 3D). Moreover, T173 of another adjacent subunit (subunit B) interacted with the Pro207 residue located at the root of the α7 – 8 using the Cγ2 atom, which is absent in the T173S mutant. Although the interaction between Ser173 and Pro207 was maintained in the structure of T173S, the N atom of Ser173, instead of Cγ2, interacted with Pro207. These facts suggest that a change in the interaction with Pro207, due to a substitution at position 173, may alter the flexibility of the α7 – 8 region in the adjacent protomer, and influence the interaction toward AcAc-CoA as a consequence.

On the other hand, kinetic analysis of the Q47L mutant showed that the mutation had an enhanced $k_{cat}/K_{M(NADPH)}$ value compared with WT PhaB, while $k_{cat}/K_{M(AcAcCoA)}$ was comparatively lower. This suggests that Q47L influenced the interaction of PhaB with NADPH. This change in kinetics was also evident by the 3-dimensional structure. Based on the crystal structure, Q47 was found to be located in the α2 helix. The loop between β2 and α2 contributed to $NADP^+$ recognition through Arg40 (Fig. 3C). Furthermore, the temperature factor in this region, as well as α7 – α8, was higher than in the others (Fig.

264 2D). These results suggest that the substitution for Q47 may alter the flexibility of this
265 region so as to be preferable for the interaction with NADP(H). Taking these results
266 together, it was concluded that the selected mutations influenced the recognition of
267 NADPH and/or AcAc-CoA indirectly via alterations in the mobility of α2 and α7 – 8. The
268 crystal structure data did account for the beneficial effects of the mutations. However, it is
269 worth noting that the mutations were unpredictable from the protein structure, which may
270 indicate the need for a combined strategy of structural and non-structural based enzyme
271 engineering.

272 The $K_{M(AcAcCoA)}$ and $K_{M(NADPH)}$ values of the native PhaB isolated from *R. eutropha*
273 were previously reported to be 5 and 19 μM, respectively (33). $K_{M(AcAcCoA)}$ was consistent
274 with the result of the present experiment, while the $K_{M(NADPH)}$ value of native PhaB was
275 lower than the recombinant protein. This disagreement in the kinetic parameters could be
276 caused by the difference in the host strain used for PhaB expression and also the presence
277 of His-tag at the N-terminal of the protein. Moreover, it is reported that *R. eutropha*
278 possesses multiple PhaB isologs (34). Therefore, the native PhaB isolated from *R. eutropha*
279 might be composed of multiple proteins having very similar physical properties, which
280 could be the cause of the differences in the kinetic parameters.

281 The potential variety in the mutated residue was estimated by the database search
282 (http://blast.ncbi.nlm.nih.gov/), which retrieved PhaB homologs assigned as AcAc-CoA
283 reductase (Fig. 4). Fig. 4 indicates alignment of PhaB homologs, which were chosen based
284 on the variety of residues 47 and 173, namely many similar sequences are omitted.
285 According to the alignment of these homologs, residue 173 was found to be located in a

286 highly-conserved region, which suggests that the region around the 173 position plays an
287 important role in PhaB activity. In contrast, the α2 region that included residue 47 was not
288 highly conserved. The position was occupied by a limited variety of amino acid residues,
289 such as Gln, Glu or Asp, but not Leu. In fact, α2 was not directly in contact with the
290 substrate and thus was presumably tolerant to further modification.
291
292 **Conclusions**
293 In this study, two novel activity-enhanced mutants of PhaB exhibited enhanced
294 $k_{cat}/K_{M(NADPH)}$ and $k_{cat}/K_{M(AcAcCoA)}$ values, respectively. The design of the plate assay-based
295 high-throughput screening, namely the effect of AACS on suppressed P(3HB) production,
296 was a key to obtaining the beneficial mutants. These mutants should be applicable to
297 obtaining higher P(3HB) production in various platforms, including microbes and plants, if
298 the monomer-supplying step is rate-limiting, as observed here for recombinant *C.*
299 *glutamicum*. In addition, the crystal structure analysis of PhaB revealed that the flexible
300 regions in PhaB contributed to the activity. The structural information reasonably explained
301 the effect of the mutations on the enzymatic activity, and provides a clue to design the
302 structure-based engineering of this enzyme, as well as future mutation/selection or other
303 strategies along similar lines to the one employed in this study.
304
305 **ACKNOWLEDGMENTS**
306 We thank Mr. John Masani Nduko for critical reading of the manuscript. This study was
307 partly supported by JSPS KAKENHI Grant Number 23310059 (to S.T.) and JST CREST

308 (to S.T.). Pacific Edit reviewed the manuscript prior to submission.

309

REFERENCES

1. **Sudesh K, K Bhubalan, JA Chuah, YK Kek, H Kamilah, N Sridewi, YF Lee.** 2011. Synthesis of polyhydroxyalkanoate from palm oil and some new applications. Appl. Microbiol. Biotechnol. **89:**1373-1386.
2. **Keshavarz T, I Roy.** 2010. Polyhydroxyalkanoates: bioplastics with a green agenda. Curr. Opin. Microbiol. **13:**321-326.
3. **Wu Q, Y Wang, GQ Chen.** 2009. Medical Application of Microbial Biopolyesters Polyhydroxyalkanoates. Artif. Cell. Blood Sub. **37:**1-12.
4. **Schubert P, A Steinbüchel, HG Schlegel.** 1988. Cloning of the *Alcaligenes eutrophus* genes for synthesis of poly-β-hydroxybutyric acid (PHB) and synthesis of PHB in *Escherichia coli*. J. Bacteriol. **170:**5837-5847.
5. **Peoples OP, AJ Sinskey.** 1989. Poly-á-hydroxybutyrate biosynthesis in Alcaligenes eutrophus H16. Characterization of the genes encoding á-ketothiolase and acetoacetyl-CoA reductase. J. Biol. Chem. **264:**15293-15297.
6. **Matsusaki H, H Abe, Y Doi.** 2000. Biosynthesis and properties of poly(3-hydroxybutyrate-*co*-3-hydroxyalkanoates) by recombinant strains of *Pseudomonas* sp. 61-3. Biomacromolecules **1:**17-22.
7. **Kichise T, T Fukui, Y Yoshida, Y Doi.** 1999. Biosynthesis of polyhydroxyalkanoates (PHA) by recombinant *Ralstonia eutropha* and effects of PHA synthase activity on *in vivo* PHA biosynthesis. Int. J. Biol. Macromol. **25:**69-77.
8. **Jung Y, J Park, Y Lee.** 2000. Metabolic engineering of *Alcaligenes eutrophus* through the transformation of cloned *phbCAB* genes for the investigation of the regulatory mechanism of polyhydroxyalkanoate biosynthesis. Enzyme Microb. Technol. **26:**201-208.
9. **Jo SJ, K Matsumoto, CR Leong, T Ooi, S Taguchi.** 2007. Improvement of poly(3-hydroxybutyrate) [P(3HB)] production in *Corynebacterium glutamicum* by codon optimization, point mutation and gene dosage of P(3HB) biosynthetic genes. J. Biosci. Bioeng. **104:**457-463.
10. **Matsumoto K, K Morimoto, A Gohda, H Shimada, S Taguchi.** 2011. Improved

polyhydroxybutyrate (PHB) production in transgenic tobacco by enhancing translation efficiency of bacterial PHB biosynthetic genes. J. Biosci. Bioeng. **111:**485-488.

11. **Taguchi S, Y Doi.** 2004. Evolution of polyhydroxyalkanoate (PHA) production system by "enzyme evolution": Successful case studies of directed evolution. Macromol. Biosci. **4:**145-156.
12. **Nomura CT, S Taguchi.** 2007. PHA synthase engineering toward superbiocatalysts for custom-made biopolymers. Appl. Microbiol. Biotechnol. **73:**969-979.
13. **Matsumoto K, S Taguchi.** 2010. Enzymatic and whole-cell synthesis of lactate-containing polyesters: toward the complete biological production of polylactate. Appl. Microbiol. Biotechnol. **85:**921-932.
14. **Taguchi S, M Yamada, K Matsumoto, K Tajima, Y Satoh, M Munekata, K Ohno, K Kohda, T Shimamura, H Kambe, S Obata.** 2008. A microbial factory for lactate-based polyesters using a lactate-polymerizing enzyme. Proc. Natl. Acad. Sci. USA **105:**17323-17327.
15. **Taguchi S, A Maehara, K Takase, M Nakahara, H Nakamura, Y Doi.** 2001. Analysis of mutational effects of a polyhydroxybutyrate (PHB) polymerase on bacterial PHB accumulation using an in vivo assay system. FEMS Microbiol. Lett. **198:**65-71.
16. **Kichise T, S Taguchi, Y Doi.** 2002. Enhanced accumulation and changed monomer composition in polyhydroxyalkanoate (PHA) copolyester by *in vitro* evolution of *Aeromonas caviae* PHA synthase. Appl. Environ. Microbiol. **68:**2411-2419.
17. **Taguchi S, H Nakamura, T Hiraishi, I Yamato, Y Doi.** 2002. In vitro evolution of a polyhydroxybutyrate synthase by intragenic suppression-type mutagenesis. J. Biochem. **131:**801-806.
18. **Okamura E, T Tomita, R Sawa, M Nishiyama, T Kuzuyama.** 2010. Unprecedented acetoacetyl-coenzyme A synthesizing enzyme of the thiolase superfamily involved in the mevalonate pathway. Proc. Natl. Acad. Sci. USA **107:**11265-11270.
19. **Matsumoto K, M Yamada, CR Leong, SJ Jo, T Kuzuyama, S Taguchi.** 2011. A new pathway for poly(3-hydroxybutyrate) production in *Escherichia coli* and *Corynebacterium glutamicum* by functional expression of a new acetoacetyl-coenzyme A synthase. Biosci. Biotechnol. Biochem. **75:**364-6.
20. **Takase K, S Taguchi, Y Doi.** 2003. Enhanced synthesis of poly(3-hydroxybutyrate) in recombinant *Escherichia coli* by means of error-prone PCR mutagenesis, saturation mutagenesis, and *in vitro* recombination of the type II polyhydroxyalkanoate synthase

gene. J. Biochem. **133:**139-145.

21. **Jo SJ, M Maeda, T Ooi, S Taguchi.** 2006. Production system for biodegradable polyester polyhydroxybutyrate by *Corynebacterium glutamicum*. J. Biosci. Bioeng. **102:**233-236.
22. **Takase K, K Matsumoto, S Taguchi, Y Doi.** 2004. Alteration of substrate chain-length specificity of type II synthase for polyhydroxyalkanoate biosynthesis by *in vitro* evolution: *in vivo* and *in vitro* enzyme assays. Biomacromolecules **5:**480-485.
23. **Kikuchi Y, M Date, K Yokoyama, Y Umezawa, H Matsui.** 2003. Secretion of active-form *Streptoverticillium mobaraense* transglutaminase by *Corynebacterium glutamicum*: Processing of the pro-transglutaminase by a cosecreted subtilisin-like protease from *Streptomyces albogriseolus*. Appl. Environ. Microbiol. **69:**358-366.
24. **Matsumoto K, F Shozui, Y Satoh, K Tajima, M Munekata, S Taguchi.** 2009. Kinetic analysis of engineered polyhydroxyalkanoate synthases with broad substrate specificity. Polym. J. **41:**237-240.
25. **Otwinowski Z, W Minor.** 1997. Processing of X-ray Diffraction Data Collected in Oscillation Mode. Methods in Enzymology **276:**307-326.
26. **Kabsch W.** 2010. Xds. Acta Crystallogr D Biol Crystallogr **66:**125-32.
27. **Vagin A, A Teplyako.** 1997. MOLREP: an automated program for molecular replacement. J. Appl. Cryst. **30:**1022-1025.
28. **Emsley P, K Cowtan.** 2004. Coot: model-building tools for molecular graphics. Acta Crystallogr D Biol Crystallogr **60:**2126-32.
29. **Murshudov GN, P Skubak, AA Lebedev, NS Pannu, RA Steiner, RA Nicholls, MD Winn, F Long, AA Vagin.** 2011. REFMAC5 for the refinement of macromolecular crystal structures. Acta Crystallogr D Biol Crystallogr **67:**355-67.
30. **Adams PD, PV Afonine, G Bunkoczi, VB Chen, IW Davis, N Echols, JJ Headd, LW Hung, GJ Kapral, RW Grosse-Kunstleve, AJ McCoy, NW Moriarty, R Oeffner, RJ Read, DC Richardson, JS Richardson, TC Terwilliger, PH Zwart.** 2010. PHENIX: a comprehensive Python-based system for macromolecular structure solution. Acta Crystallogr D Biol Crystallogr **66:**213-21.
31. **Song YY, K Matsumoto, M Yamada, A Gohda, CJ Brigham, AJ Sinskey, S Taguchi.** 2012. Engineered *Corynebacterium glutamicum* as an endotoxin-free platform strain for lactate-based polyester production. Appl. Microbiol. Biotechnol. **93:**1917-1925.
32. **Price AC, YM Zhang, CO Rock, SW White.** 2004. Cofactor-induced conformational

rearrangements establish a catalytically competent active site and a proton relay conduit in FabG. Structure **12:**417-428.

33. **Haywood GW, AJ Anderson, L Chu, EA Dawes.** 1988. The role of NADH- and NADPH-linked acetoacetyl-CoA reducatses in the poly-3-hydroxybutyrate synthesizing organism *Alcaligenes eutrophus* FEMS Microbiol.Lett. **52:**259-264.
34. **Budde CF, AE Mahan, JN Lu, C Rha, AJ Sinskey.** 2010. Roles of multiple acetoacetyl Coenzyme A reductases in polyhydroxybutyrate biosynthesis in *Ralstonia eutropha* H16. J. Bacteriol. **192:**5319-5328.

FIGURE LEGENDS

FIG. 1. P(3HB) production in recombinant *C. glutamicum* harboring the engineered *phaB* genes. (A) Time course of P(3HB) accumulation. Circle: wild-type PhaB, triangle: Q47L, square: T173S. (B) Correlation between the enzymatic activity and P(3HB) content in recombinant *C. glutamicum*. Black bar: enzymatic activity (left axis). Gray bar: P(3HB) content (right axis). The PhaB activity was measured at 24 h. All data is the average of at least three trials.

FIG. 2. Crystal structure of the PhaB and mutants. (A) Ribbon diagram of the PhaB monomer. The ribbon model is colored according to the sequence, from blue at the N-terminus to red at the C-terminus. (B) Tetrameric structure of PhaB. The model is colored according to the subunit. Q47 (purple) and T137 (cyan) are also shown as spherical models. (C) Structure superimposition among wild-type (red), Q47L (blue), and T137S (orange). For clarity, only a monomer of the superimposed tetramer is shown. (D) Temperature factor of wild type PhaB. The tube model is colored according to the

temperature factor, from blue at 20 to red at 50. The width of the tube also corresponds to temperature factor. In short, red thick region implies high flexibility and blue thin region low. Q47 is also shown as green sticks. The flexible α7 - 8 and α2 are indicated.

FIG. 3. Crystal structure of PhaB – AcAc-CoA – $NADP^+$ ternary complex. (A) The Fo-Fc map (contoured at 1.5s) of AcAc-CoA and $NADP^+$. AcAc-CoA (yellow) and $NADP^+$ (green) are also shown as sticks. (B) Ribbon diagram of the tetramer in complex with AcAc-CoA and $NADP^+$. The bound AcAc-CoA (yellow) and $NADP^+$ (green) are shown as spherical models. (C) Close-up view of the substrate-binding site. The bound substrates and their recognition residues are shown in stick models. The flexible α7 – 8 region and β2 – α2 are colored purple and brown, respectively. (D) T173 in the adjacent subunits located around the AcAc-CoA binding site. T173 residues in the adjacent subunits are shown as blue spheres. P207 interacting with T173 is shown as a purple sphere. The ribbon diagrams are colored according to the subunits, although the flexible α7 – 8 regions and their continuing loops are colored purple.

FIG. 4. Partial alignment of PhaB from *R. eutropha* and its homologous enzymes. Asterisk indicates the beneficial sites. Secondary structure was shown based on the crystal structure of PhaB from *R. eutropha*. The residue 47 locates in the non-conserved α-helix, while residue 173 locates in the random coil. The position 47 is often occupied with hydrophilic residues. The position 173 is mostly occupied with Thr, while some PhaB homologs possess Ser residue at this position.

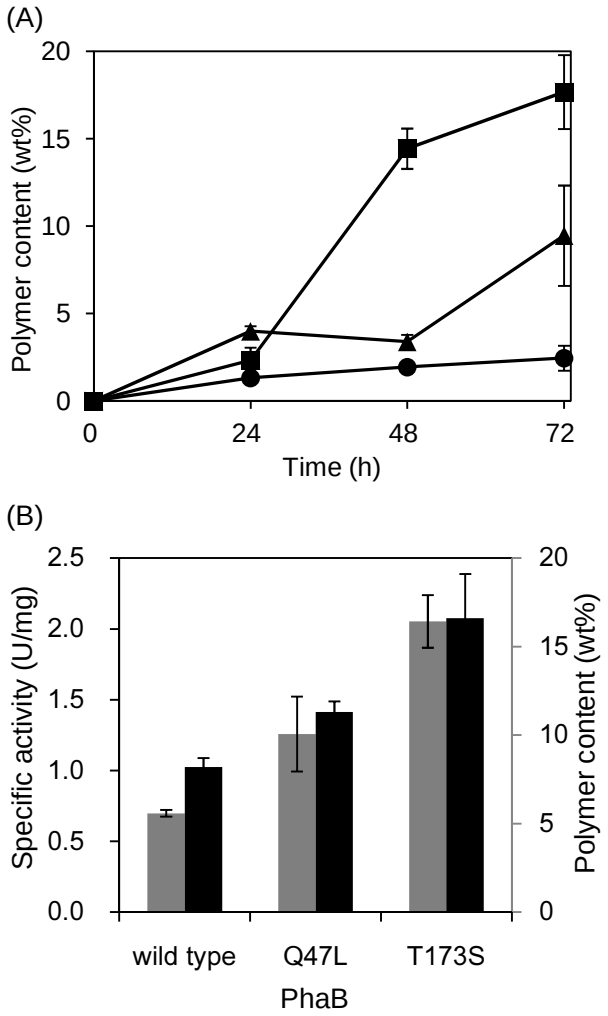
(A)
Polymer content (wt%)
20
15
10
5
0
0
24
48
72
Time (h)
(B)
Specific activity (U/mg)
2.5
2.0
1.5
1.0
0.5
0.0
20
15
10
5
0
Polymer content (wt%)
wild type
Q47L
T173S
PhaB

Figure 1

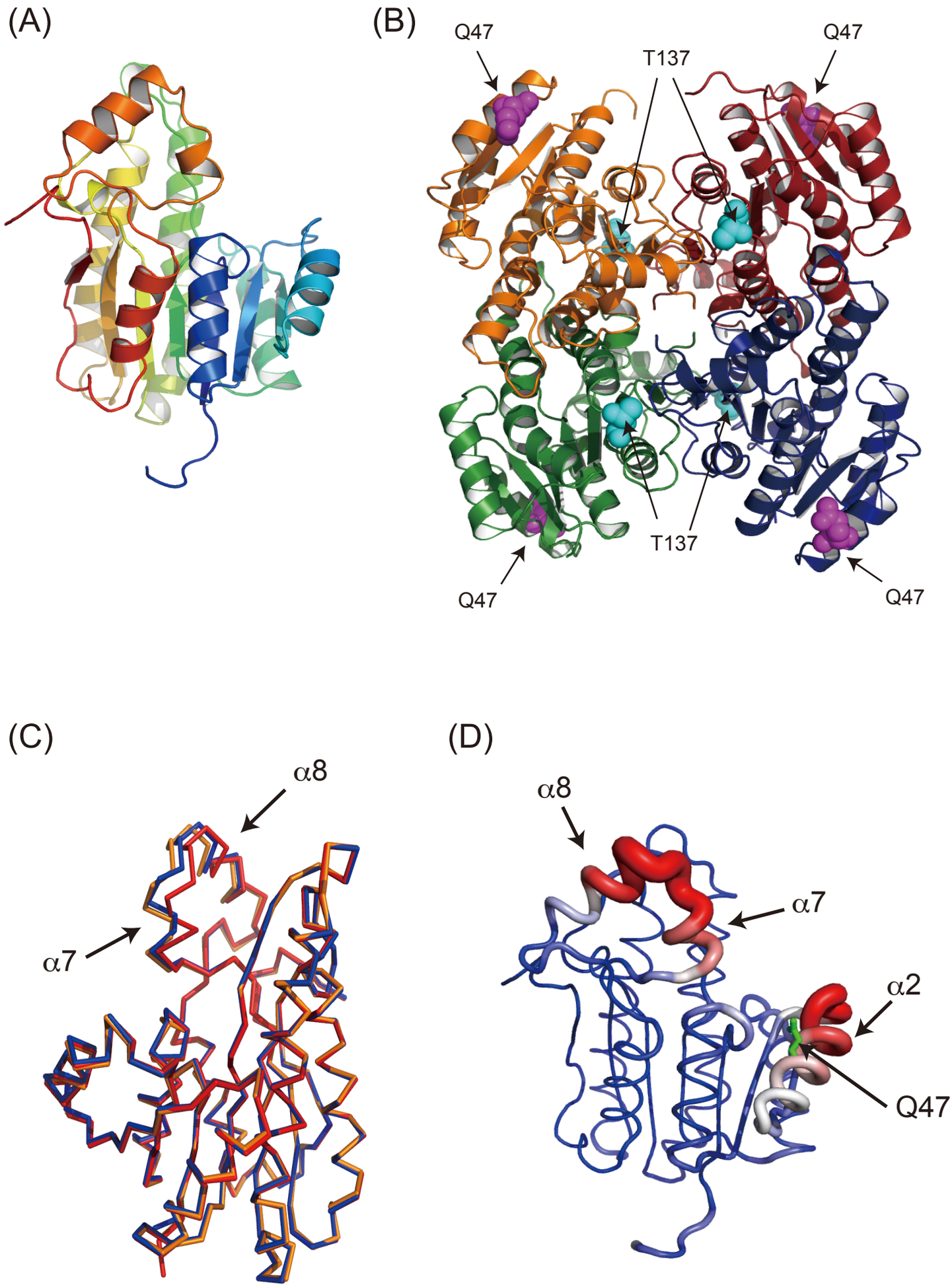

Fig. 2

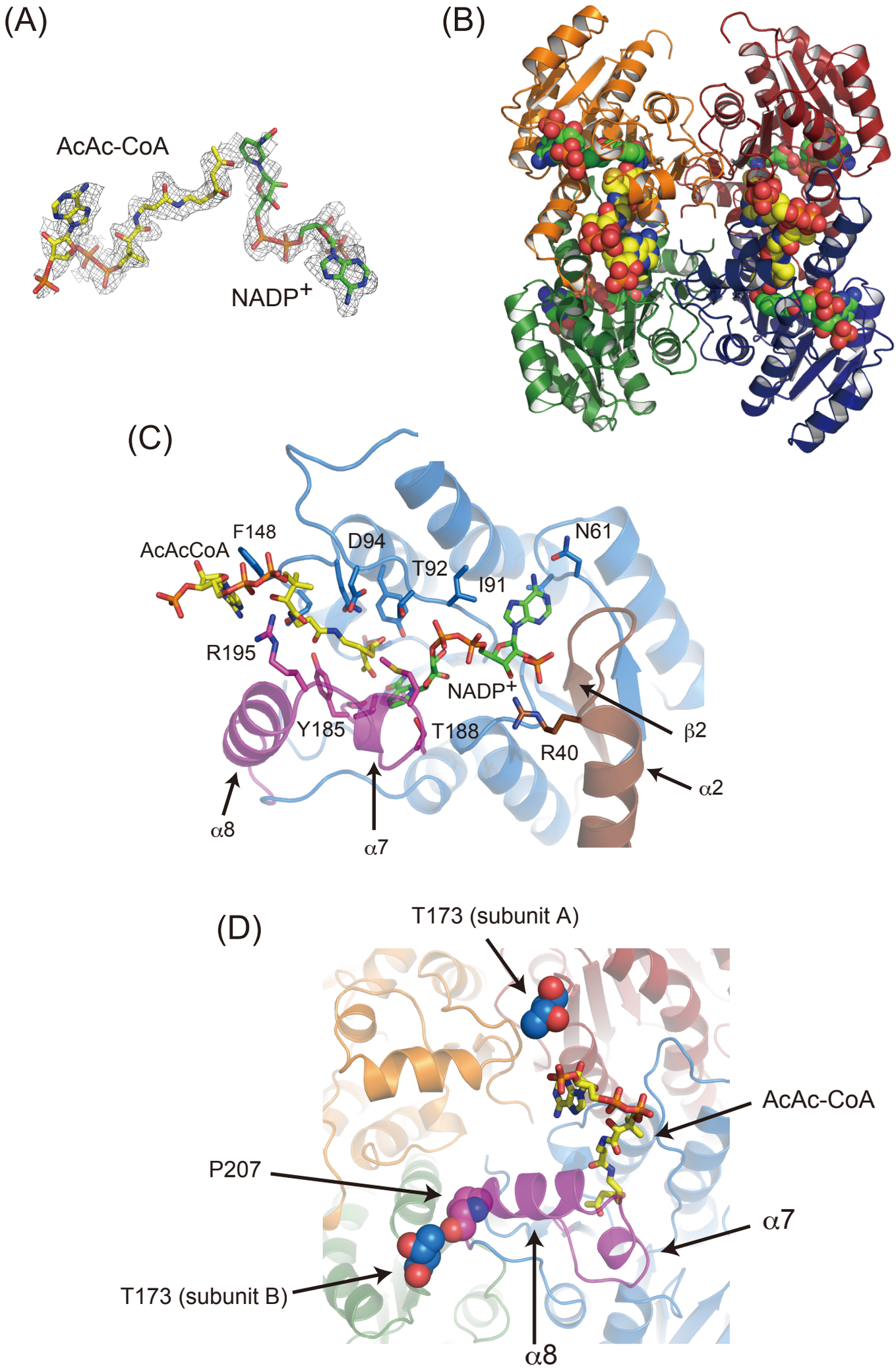
(A)
AcAc-CoA
NADP+
(B)
(C)
AcAcCoA
F148
D94
N61
T92
I91
R195
NADP+
Y185
T188
R40
β2
α2
α8
α7
(D)
T173 (subunit A)
AcAc-CoA
P207
α7
T173 (subunit B)
α8

Fig. 3

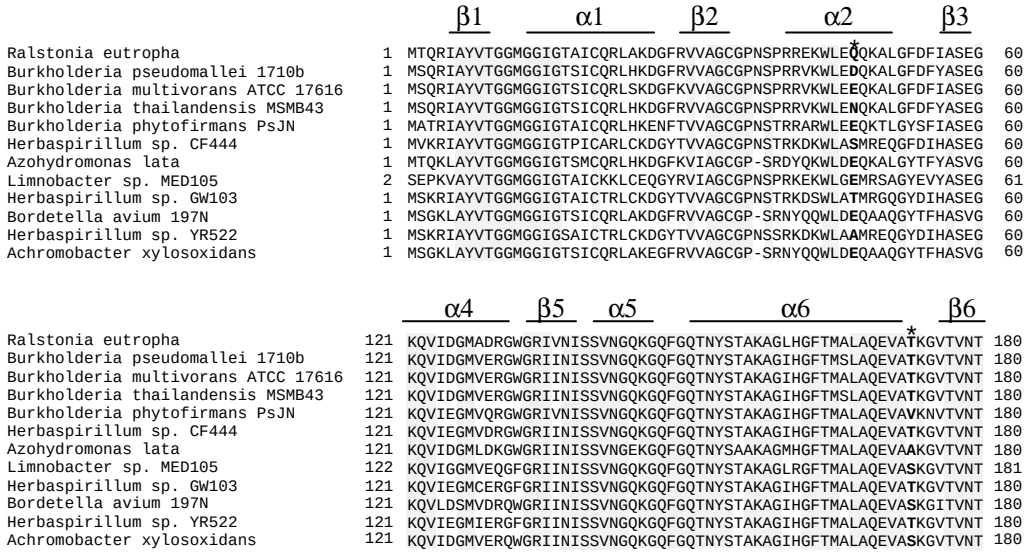
β1 α1 β2 α2 β3
Ralstonia eutropha 1 MTQRIAYVTGGMGGIGTAICQRLAKDGFRVVAGCGPNSPRREKWLEQQKALGFDFIASEG 60
Burkholderia pseudomallei 1710b 1 MSQRIAYVTGGMGGIGTSICQRLHKDGFRVVAGCGPNSPRRVKWLEDQKALGFDFYASEG 60
Burkholderia multivorans ATCC 17616 1 MSQRIAYVTGGMGGIGTSICQRLSKDGFKVVAGCGPNSPRRVKWLEEQKALGFDFIASEG 60
Burkholderia thailandensis MSMB43 1 MSQRIAYVTGGMGGIGTSICQRLHKDGFRVVAGCGPNSPRRVKWLENQKALGFDFYASEG 60
Burkholderia phytofirmans PsJN 1 MATRIAYVTGGMGGIGTAICQRLHKENFTVVAGCGPNSTRRARWLEEQKTLGYSFIASEG 60
Herbaspirillum sp. CF444 1 MVKRIAYVTGGMGGIGTPICARLCKDGYTVVAGCGPNSTRKDKWLASMREQGFDIHASEG 60
Azohydromonas lata 1 MTQKLAYVTGGMGGIGTSMCQRLHKDGFKVIAGCGP-SRDYQKWLDEQKALGYTFYASVG 60
Limnobacter sp. MED105 2 SEPKVAYVTGGMGGIGTAICKKLCEQGYRVIAGCGPNSPRKEKWLGEMRSAGYEVYASEG 61
Herbaspirillum sp. GW103 1 MSKRIAYVTGGMGGIGTAICTRLCKDGYTVVAGCGPNSTRKDSWLATMRGQGYDIHASEG 60
Bordetella avium 197N 1 MSGKLAYVTGGMGGIGTSICQRLAKDGFRVVAGCGP-SRNYQQWLDEQAAQGYTFHASVG 60
Herbaspirillum sp. YR522 1 MSKRIAYVTGGMGGIGSAICTRLCKDGYTVVAGCGPNSSRKDKWLAAMREQGYDIHASEG 60
Achromobacter xylosoxidans 1 MSGKLAYVTGGMGGIGTSICQRLAKEGFRVVAGCGP-SRNYQQWLDEQAAQGYTFHASVG 60
α4 β5 α5 α6 β6
Ralstonia eutropha 121 KQVIDGMADRGWGRIVNISSVNGQKGQFGQTNYSTAKAGLHGFTMALAQEVATKGVTVNT 180
Burkholderia pseudomallei 1710b 121 KQVIDGMVERGWGRIINISSVNGQKGQFGQTNYSTAKAGIHGFTMSLAQEVATKGVTVNT 180
Burkholderia multivorans ATCC 17616 121 KQVIDGMVERGWGRIINISSVNGQKGQFGQTNYSTAKAGIHGFTMALAQEVATKGVTVNT 180
Burkholderia thailandensis MSMB43 121 KQVIDGMVERGWGRIINISSVNGQKGQFGQTNYSTAKAGIHGFTMSLAQEVATKGVTVNT 180
Burkholderia phytofirmans PsJN 121 KQVIEGMVQRGWGRIVNISSVNGQKGQFGQTNYSTAKAGIHGFTMALAQEVAVKNVTVNT 180
Herbaspirillum sp. CF444 121 KQVIEGMVDRGWGRIINISSVNGQKGQFGQTNYSTAKAGIHGFTMALAQEVATKGVTVNT 180
Azohydromonas lata 121 KQVIDGMLDKGWGRIINISSVNGEKGQFGQTNYSAAKAGMHGFTMALAQEVAAKGVTVNT 180
Limnobacter sp. MED105 122 KQVIGGMVEQGFGRIINISSVNGQKGQFGQTNYSTAKAGLRGFTMALAQEVASKGVTVNT 181
Herbaspirillum sp. GW103 121 KQVIEGMCERGFGRIINISSVNGQKGQFGQTNYSTAKAGIHGFTMALAQEVATKGVTVNT 180
Bordetella avium 197N 121 KQVLDSMVDRQWGRIINISSVNGQKGQFGQTNYSTAKAGIHGFTMALAQEVASKGITVNT 180
Herbaspirillum sp. YR522 121 KQVIEGMIERGFGRIINISSVNGQKGQFGQTNYSTAKAGIHGFTMALAQEVATKGVTVNT 180
Achromobacter xylosoxidans 121 KQVIDGMVERQWGRIINISSVNGQKGQFGQTNYSTAKAGIHGFTMALAQEVASKGVTVNT 180

Figure 4.

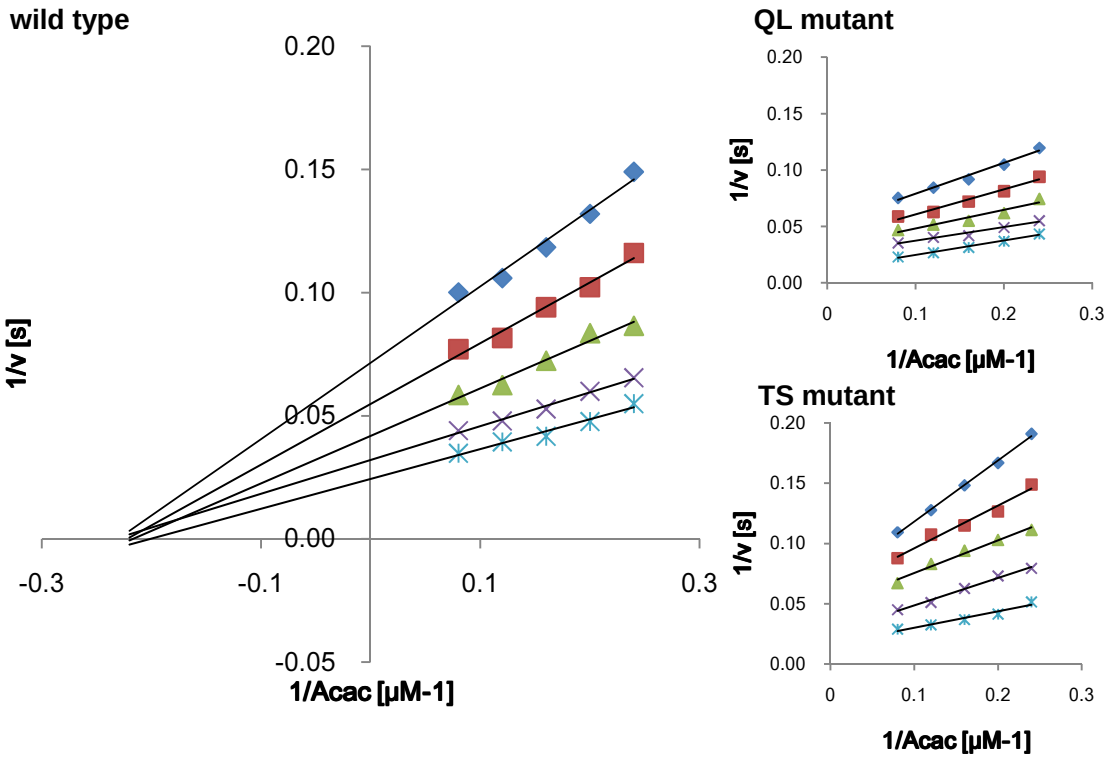

Figure S1. Lineweaver Burk plots for the wild-type and mutated acetoacetyl-CoA reductase (PhaB). NADPH concentrations are 25 (diamond), 31 (square), 42 (triangle), 62.5 (cross) and 125 µM (asterisk), respectively.

Table S1. X-ray data collection and refinement statistics

	wild type	Q47L	T137S	ternary complex
PDB ID	3VZP	3VZQ	3VZR	3VZS
Data collection				
Beamline	Photon Factory BL1A	In house (RIGAKU R-AXIS IV)	Spring-8 BL41XU	Photon Factory BL5A
Wavelength	1.0000	1.5418	1.0000	1.0000
Resolution range* (Å)	20.06 - 1.79 (1.90 - 1.79)	45.3 - 2.00 (2.12 - 2.00)	20.00 - 2.90 (3.00 - 2.90)	50.00 - 2.14 (2.18 - 2.14)
Space group	$C222_1$	$C2$	$C222_1$	$C222_1$
Unit-cell parameters (Å, °)	a = 67.7, b =123.7, c = 260.8	a = 93.6, b =88.6, c = 70.7, β = 104.24	a =70.7, b =185.9, c = 75.5	a = 67.4, b =123.4, c = 260.2
Number of molecule in an asymmetric unit	4	2	2	4
No. of observed reflections	721056	159130	67176	330241
No. of unique reflections	100490	37627	11342	58459
Multiplicity*	7.18 (6.98)	4.23 (4.08)	5.9 (4.8)	5.6 (6.2)
Completeness * (%)	97.7 (89.2)	99.4 (97.8)	99.8 (99.3)	96.9 (98.7)
$<I>/<\sigma(I)>$*	17.85 (3.86)	7.07 (3.07)	7.57 (2.15)	25.14 (7.86)
R_{sym}* (%)	10.1 (61.8)	16.1 (43.4)	17.9 (51.4)	9.1 (30.3)
Refinement				
R-factor / R-free (%)	19.2 / 23.8	23.5 / 26.7	18.9 / 24.0	16.2 / 20.7
No. of atoms	8195	4075	3668	8469
proten	7414	3668	3668	7414
ligands	89	0	0	428
water	692	407	0	627
R.m.s.d bond lengths (Å)	0.007	0.002	0.005	0.003
R.m.s.d bond angles (°)	0.98	0.61	0.84	0.77
Average B-factor	21.3	14.0	24.3	19.6
Ramachandran plot† (%)				
favored	98	98	97	98
ouliers	0	0	0	0

*Values in parentheses are for outermost shell.

†Ramachandran statistics were calculated with MolProbity.